Electronic Supplementary Material (ESI) for CrystEngComm.

Benzene-1,3,5-tricarboxamide *n*-alkyl ester and carboxylic acid derivatives: Tuneable structural, morphological and thermal properties

Amy D. Lynes,[a*] Chris S. Hawes,[a] Edward N. Ward,[b] Benjamin Haffner,[c] Matthias Mobius,[c] Kevin Byrne,[d] Wolfgang Schmitt,[d] Robert Pal[b] and Thorfinnur Gunnlaugsson[a*]

[a]School of Chemistry and Trinity Biomedical Sciences Insitute (TBSI), The University of Dublin, Trinity College Dublin, Dublin 2, Ireland. gunnlaut@tcd.ie; lynesa@tcd.ie

[b]Department of Chemistry, Durham University, South Road, Durham, DH1 3LE (UK)

[c]Sami Nasr Institute of Advanced Materials (SNIAM), School of Physics, The University of Dublin, Trinity College Dublin, Dublin 2, Ireland

[d]School of Chemistry, Centre for Research on Adaptive Nanostructures and Nanodevices (CRANN), The University of Dublin, Trinity College Dublin, Dublin 2, Ireland

Supporting Information

Synthesis of Alkylamine Precursors

Synthesis of methyl 5-aminopentanoate and methyl 6-aminohexanoate
The appropriate amino acid (21 mmol) was dissolved in 100 ml of CH_3OH and cooled in ice, before addition of 5 equivalents of $SOCl_2$ dropwise. The mixture was stirred for 12 hours at room temperature. $SOCl_2$ and CH_3OH were removed by vacuum distillation to reveal a powdery white solid in each case, which was dried *in vacuo*.

Methyl 5-aminopentanoate, yield 86%; mp 132-136 ˚C (lit.[S1] 132-137˚C). 1H NMR (DMSO-d6, 400 MHz, δ) 7.95 (s, 2H, NH2), 3.59 (s, 3H, COOMe), 2.76 (m, 2H, 1-CH2), 2.39-2.28 (m, 2H, 4- CH_2), 1.48 (m, 4H, 2-CH_2, 3-CH_2). ^{13}C NMR (DMSO-d_6, 150 Hz, δ) 173.08 (COOMe), 51.27 (Me), 38.37 (C1), 32.65 (C4), 26.36 (C2), 21.35 (C3). HRMS-ESI$^+$ (*m/z)* : $[M+H]^+$ calcd for $C_6H_{14}NO_2$, 132.1025, found 132.1030. IR ν_{max} (cm^{-1}): 3024s, 2931s, 1734s, 1597m, 1575m, 1518m, 1474w, 1443m, 1420m, 1385m, 1345s, 1270s, 1192s, 1149s, 1149s, 1054m, 1022w, 982m, 949m, 899m, 882m, 747s, 700w, 586w.

Methyl 6-aminohexanoate, yield 98%**;** mp 80-84 ˚C (lit.[S2] mp 81-82˚C) ^{1}H NMR (DMSO-d_6, 400 MHz, δ) 7.92 (s, 2H, NH_2), 3.58 (s, 3H, COOMe), 2.74 (m, 2H, 1-CH_2), 2.30 (t, J = 7.3 Hz, 2H, 5-CH_2), 1.54 (m, 4H, 2-CH_2, 4-CH_2), 1.3 (q, J = 8.0 Hz, 2H, 3-CH_2). ^{13}C NMR (DMSO-d_6, 150 Hz, δ) 173.22 (COOMe), 51.23 (Me), 38.50 (C1), 33.02 (C5), 26.59 (C2), 25.27 (C4), 23.87 (C3). HRMS-ESI$^+$ (*m/z)* : $[M+H]^+$ calcd for $C_7H_{16}NO_2$, 146.1103, found 146.1171. IR ν_{max} (cm^{-1}): 3019s, 2927s, 2865s, 1726s, 1627m, 1603w, 1583m, 1496m, 1425w, 1395w, 1363m, 1313m, 1228s, 1192s, 1143s, 1094s, 1045m, 977m, 949w, 931w, 832m, 812m, 731m, 703w, 611m.

2. Gel Photographs

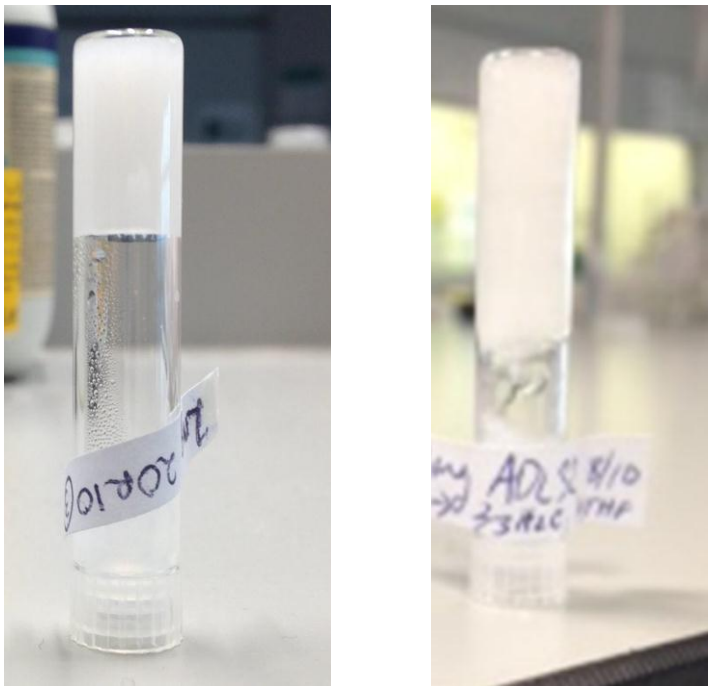

Figure S1 Inversion test for THF/H_2O gels of compound **5** (left) and **3** (right).

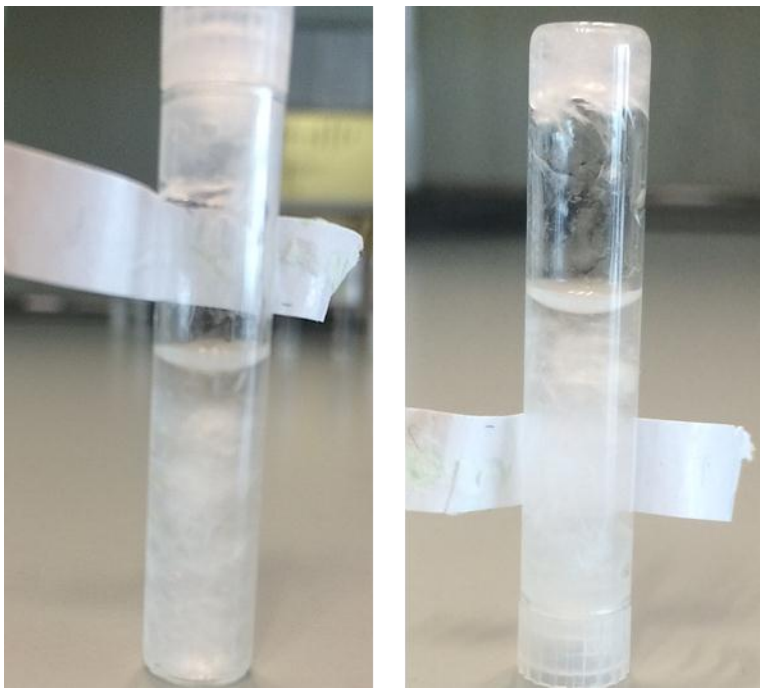

Figure S2 Weak gel and failed inversion test with compound **1**.

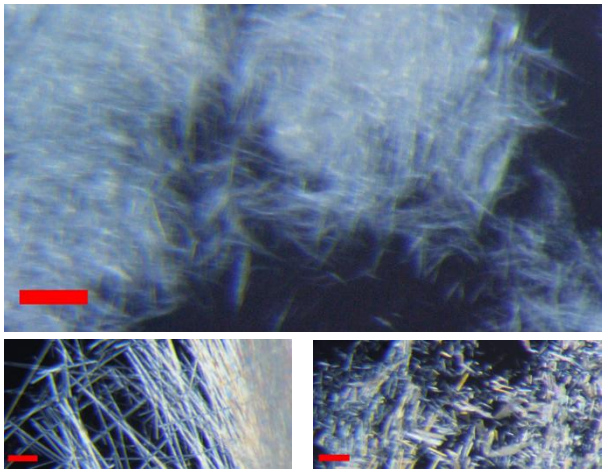

Figure S3 Polarised Optical microscopy for compounds **5** (top), **3** (bottom left) and **1** (bottom right) (all scale bars 100 μm).

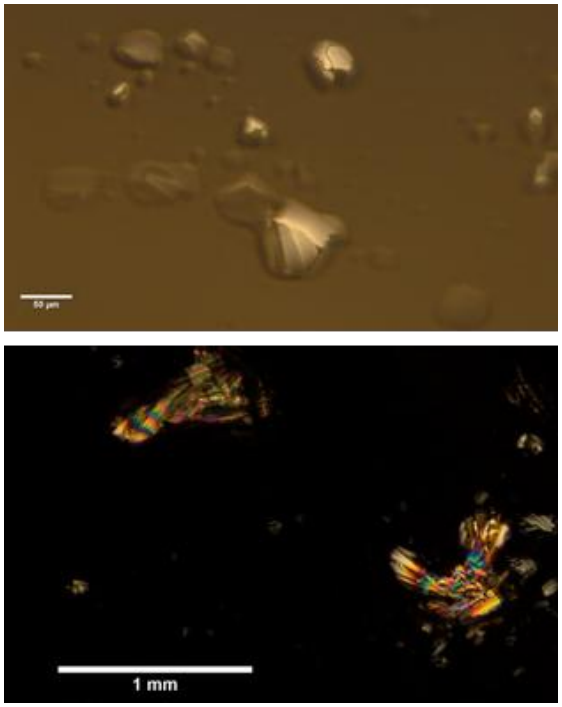

Figure S4 Polarised optical microscopy (cooling cycle) of **2** at 72.9 °C (top, scale bar 50 μm) and 62.7 °C (bottom).

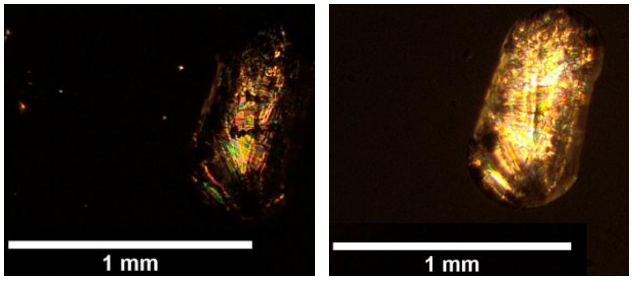

Figure S5 Polarised optical microscopy (cooling cycle) of **4** at 102.9 °C (left) and at 56 °C (right).

3. Thermogravimetric Analysis

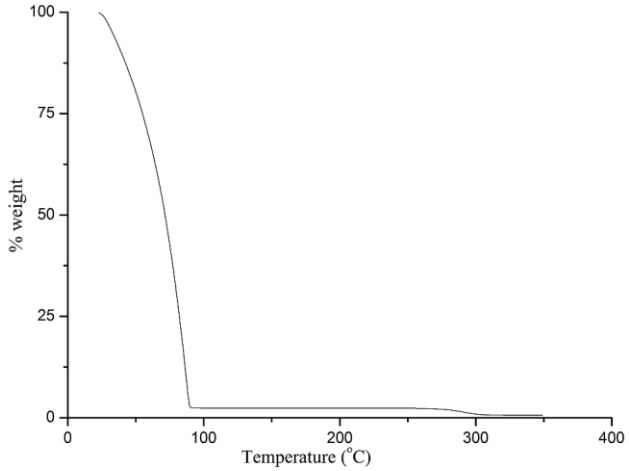

Figure S6 Thermogravimetric analysis plot of gel **1**

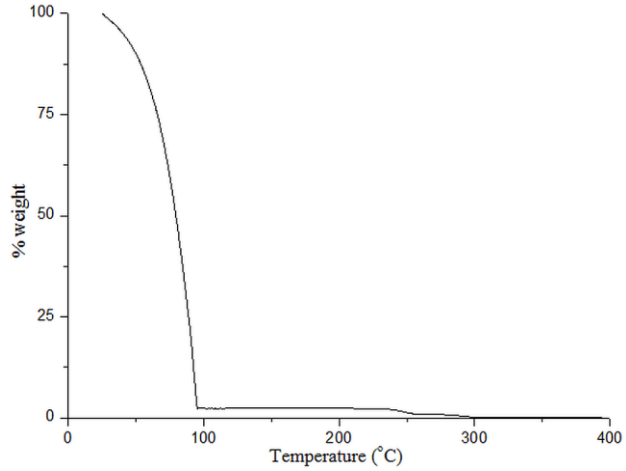

Figure S7 Thermogravimetric analysis plot of gel **3**

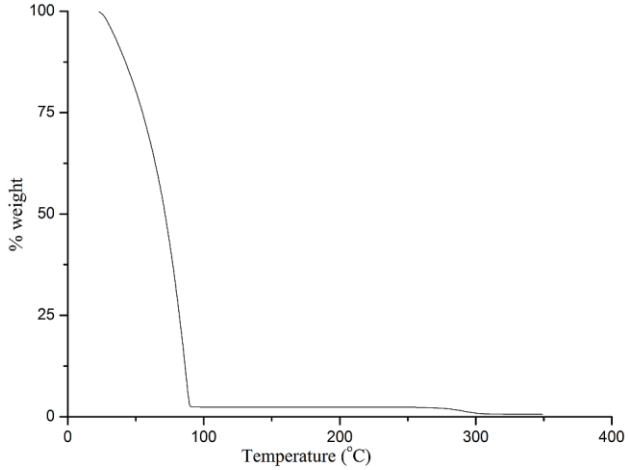

Figure S8 Thermogravimetric analysis plot of gel **5** (as synthesised)

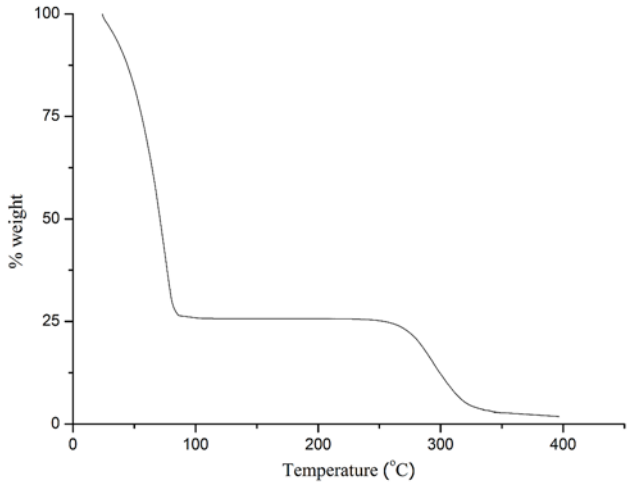

Figure S9 Thermogravimetric analysis plot of gel **5** following compression and rheology experiments

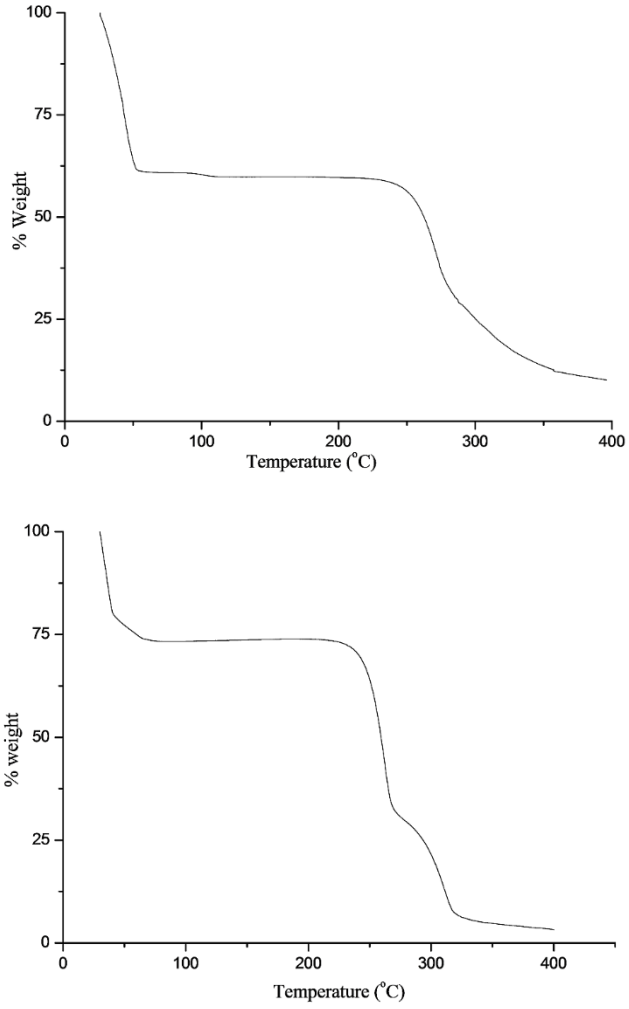

Figure S10 Thermogravimetric analysis plots of crystalline samples of compounds **1** (top) and **3** (bottom).

4. Differential Scanning Calorimetry

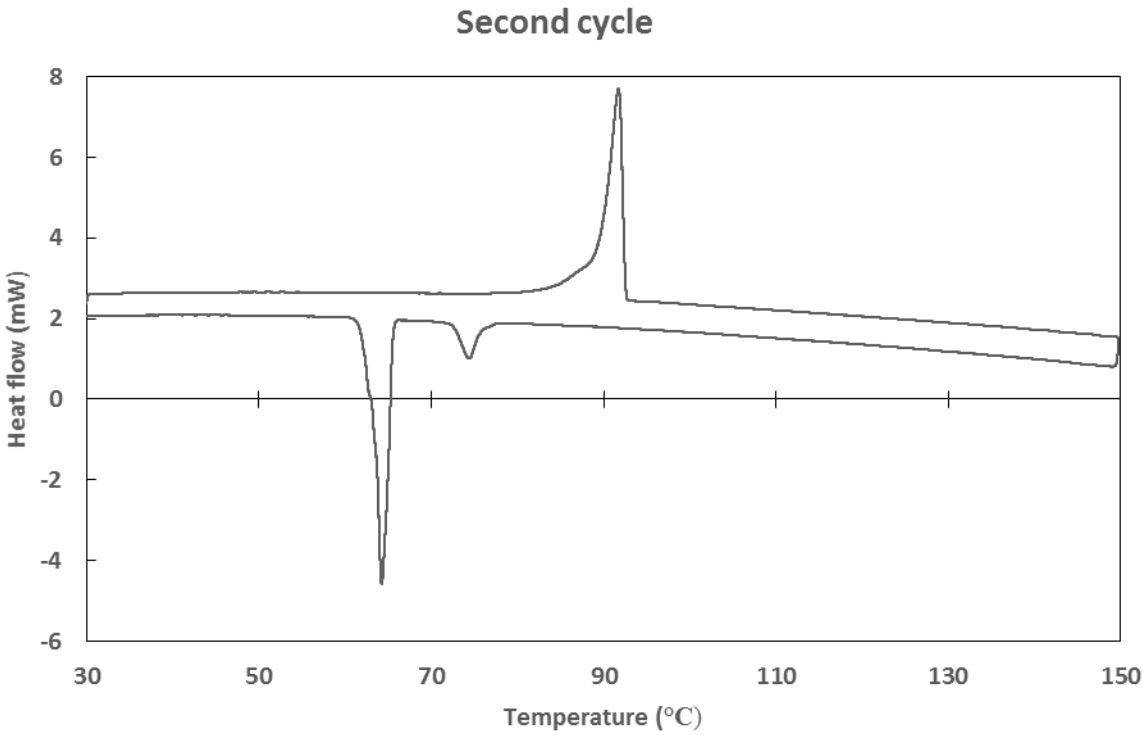

Figure S11 DSC thermograph of **2** displaying an endothermic transition onset at 81.6 °C and exothermic transitions onset at 71.5 °C and 60.6 °C

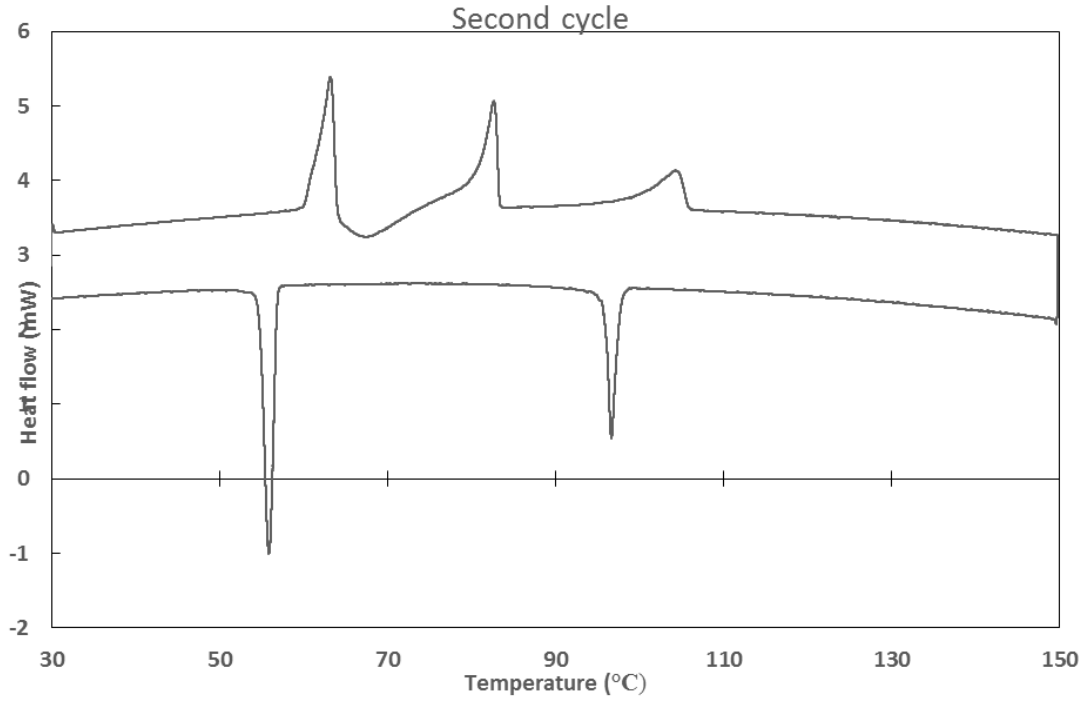

Figure S12 DSC thermograph of **4** showing endothermic transitions onset at 59.3, 75.1 and 95.5 °C and exothermic transitions at 98.6 and 57.2 °C

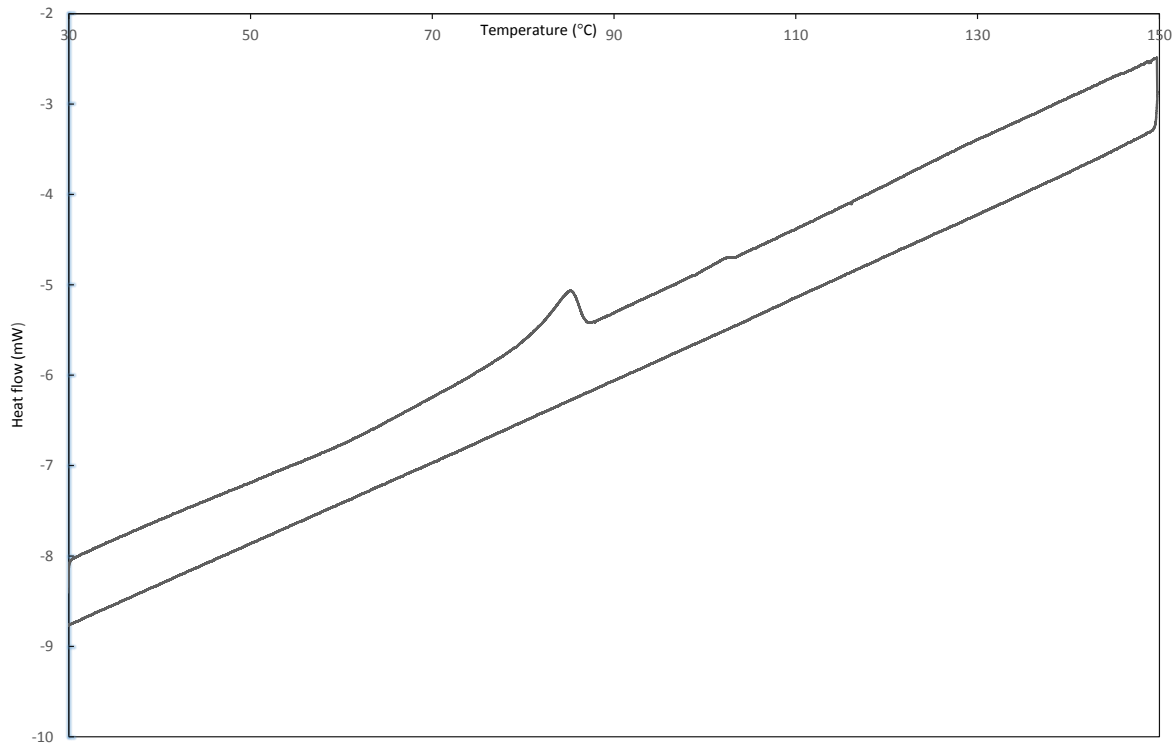

Figure S13 DSC thermograph of **Me_3-1**

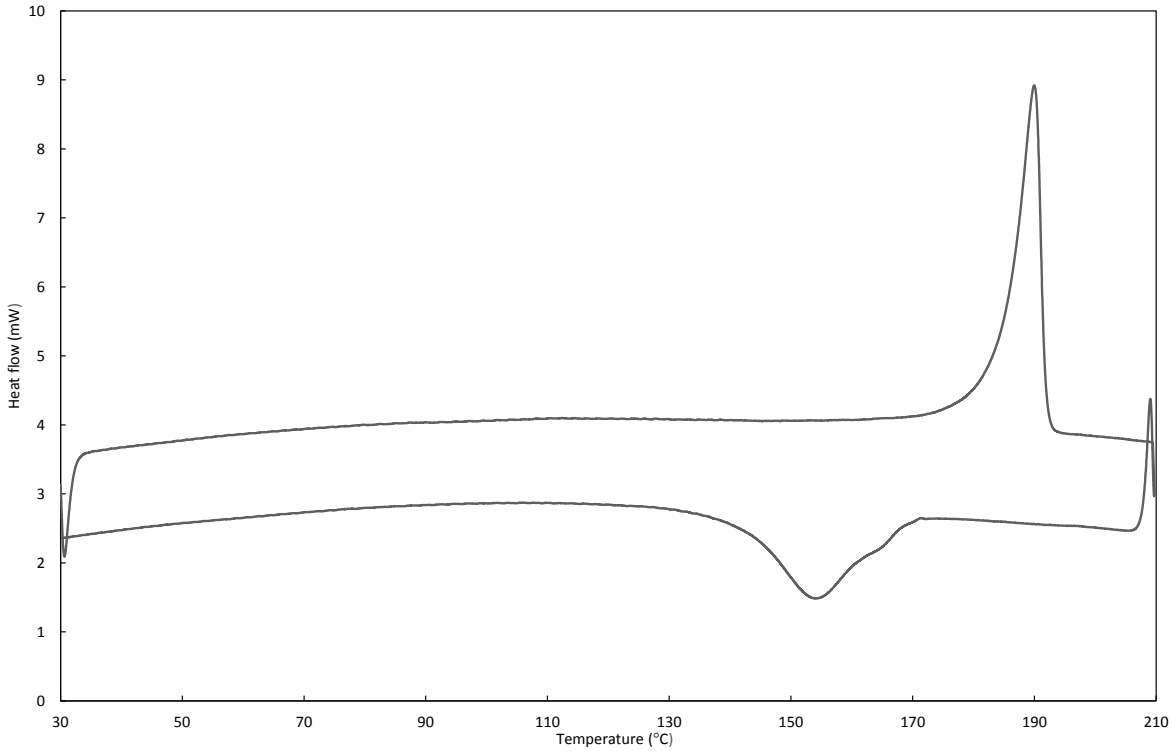

Figure S14 DSC thermograph of compound **1**

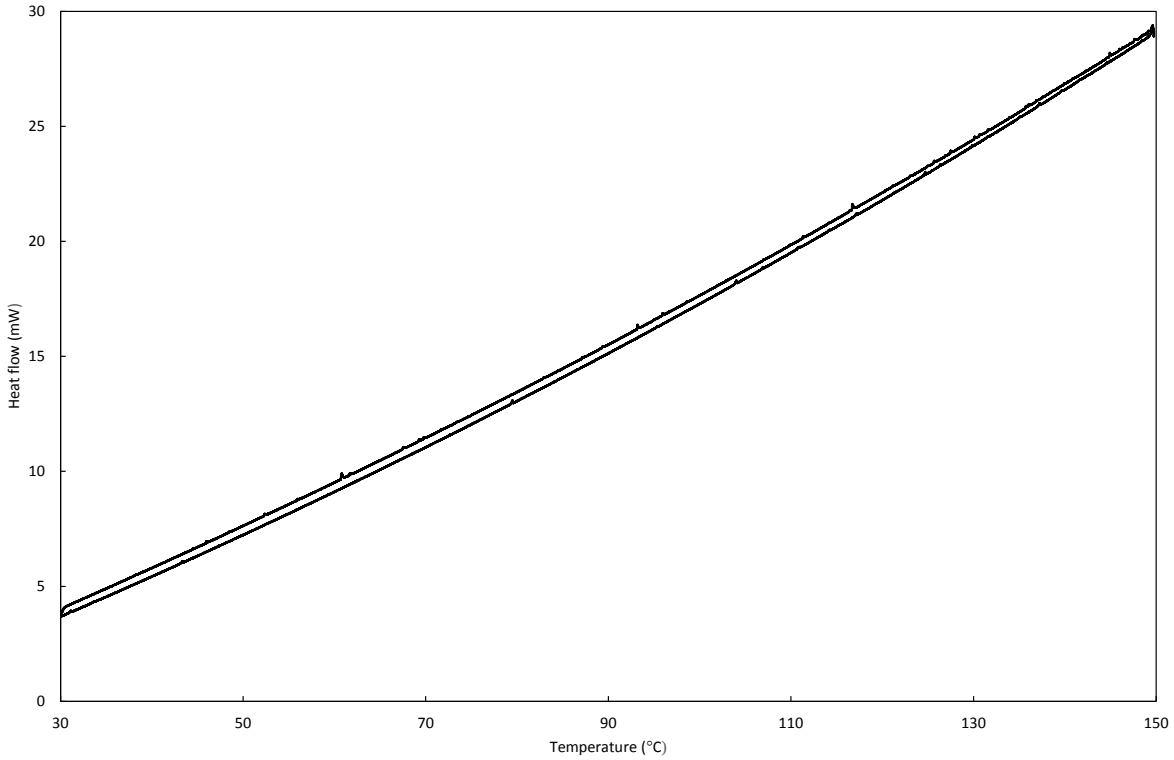

Figure S15 DSC Thermograph of compound **3**

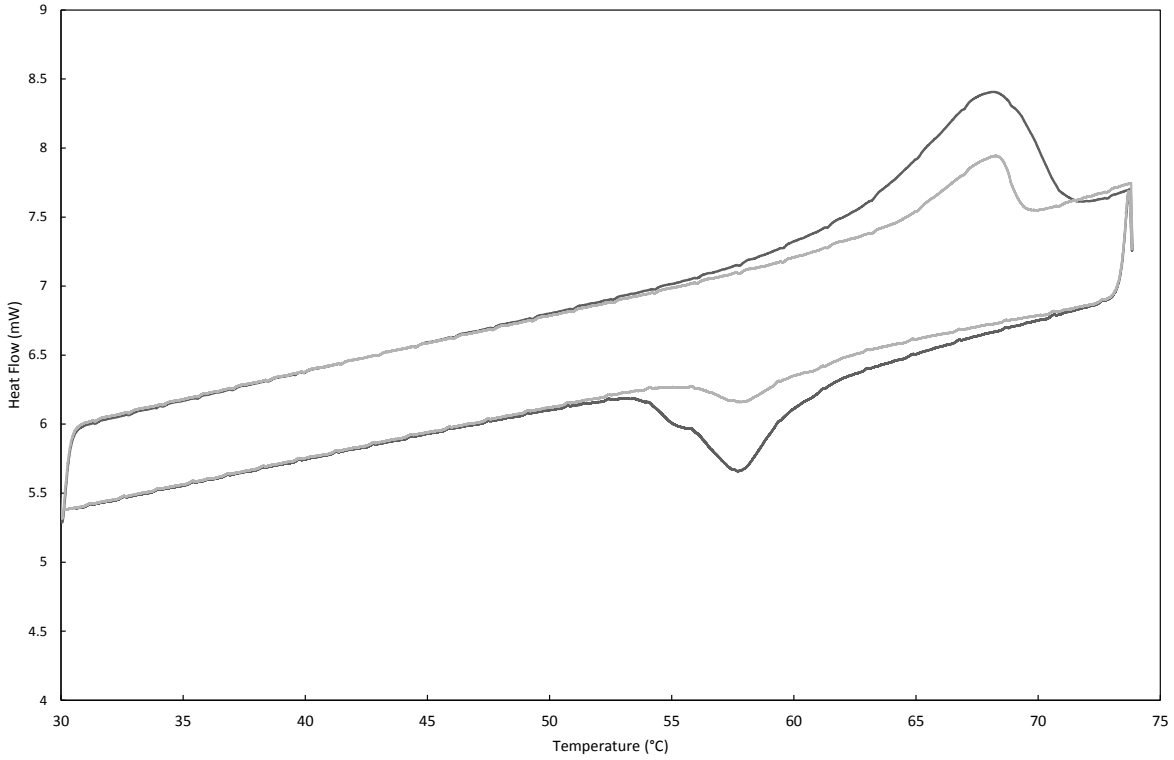

Figure S16 DSC thermograph of compound **4** showing two sequential cycles 30 – 74 °C showing diminishing of the first phase transition on sequential heating and cooling cycles.

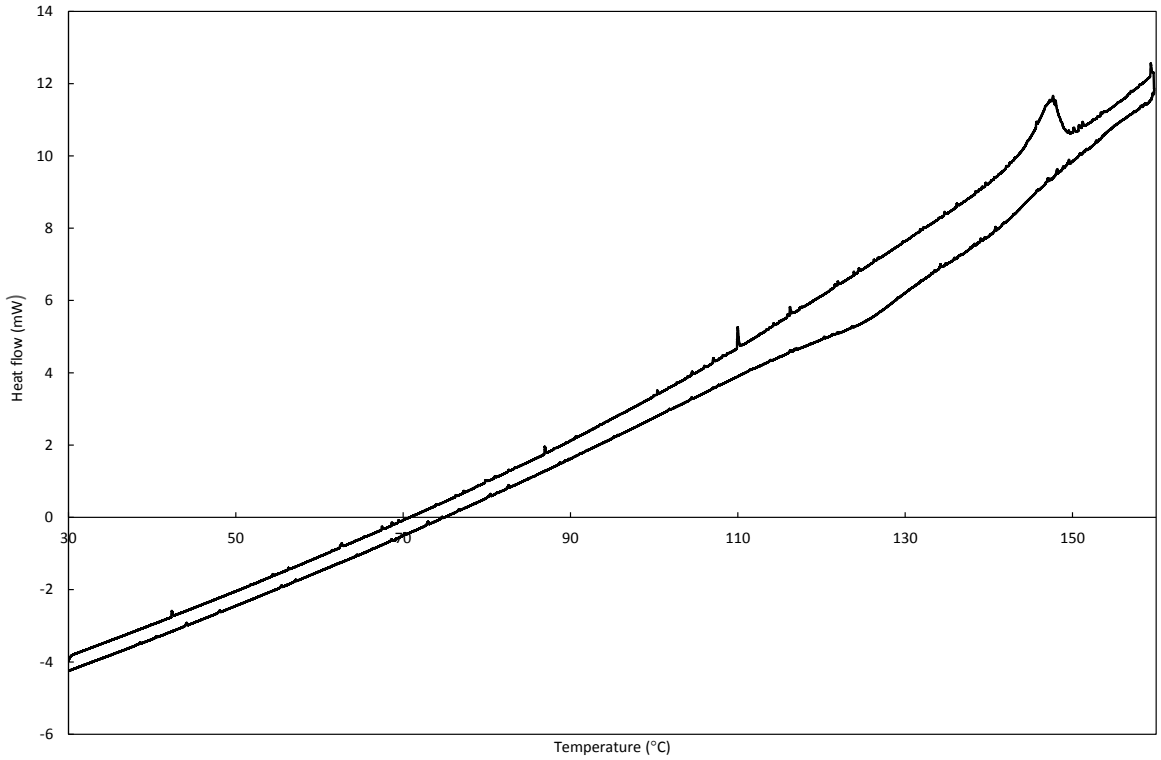

Figure S17 DSC Thermograph of compound **5**

5. X-ray Powder Diffraction

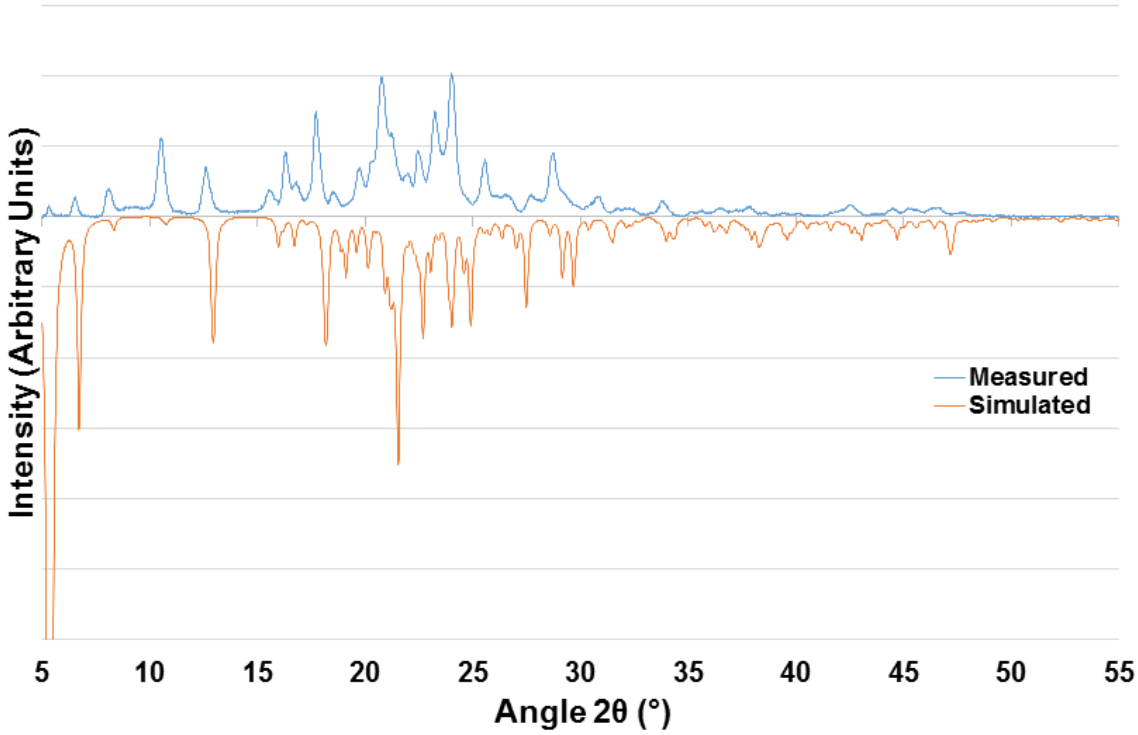

Figure S18 X-ray powder diffraction pattern for compound **1**, measured at room temperature, compared to the simulated pattern from the single-crystal data collected at 100K. To account for preferred orientation caused by the needle-like crystallite morphology, the data were simulated with preferred orientation (011) with March-Dollase parameter of 2.

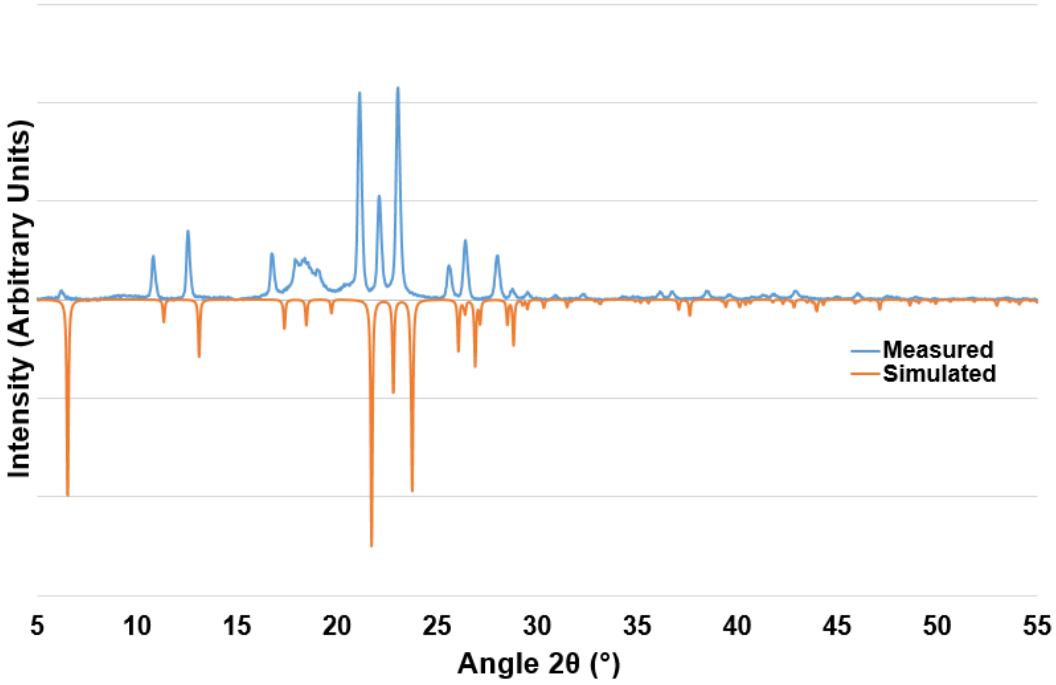

Figure S19 X-ray powder diffraction pattern of compound **2** collected at room temperature compared to the simulated pattern from the single crystal data collected at 100K.

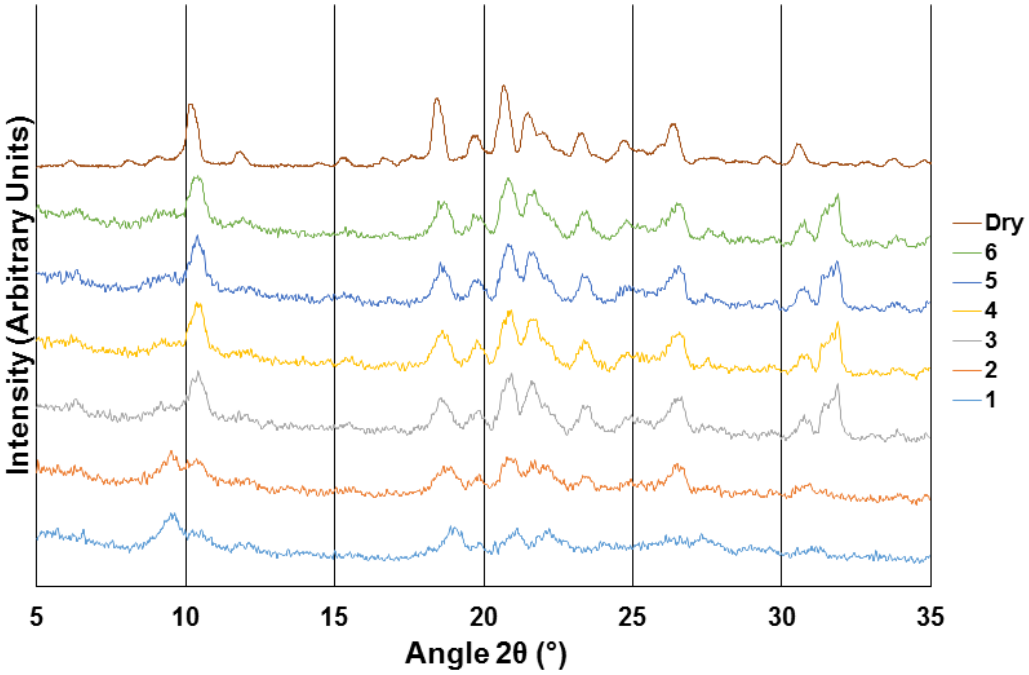

Figure S20 Sequential X-ray powder diffraction patterns for compound **3** collected immediately after removal of the crystals from the recrystallization solvent, showing the rapid loss of the original poorly-crystalline phase and growth of the collapsed microcrystalline phase. Each of the scans 1 – 6 corresponds to 3 minutes exposure. The dry sample was measured after drying the sample *in vacuo* with 30 minute exposure time.

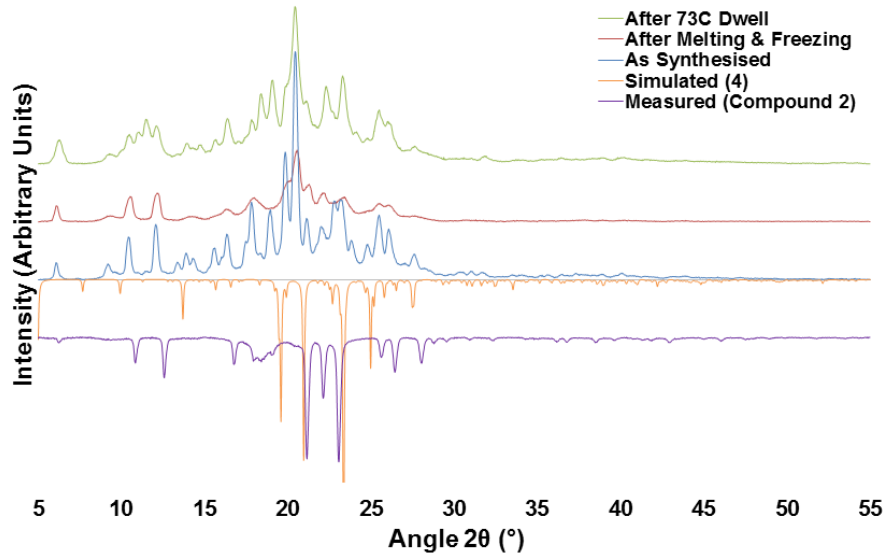

Figure S21 X-ray powder diffraction pattern for compound **4** (room temperature), showing the as-synthesised material consisting of multiple crystalline and polycrystalline phases (blue); the single, poorly-crystalline phase obtained by complete melting and freezing of the material (red); the mixture of at least two phases obtained by heating above the first phase transition temperature (green), and comparison with the simulated pattern for compound **4** (orange) and the measured pattern for compound **2** (purple).

6. NMR Spectroscopy

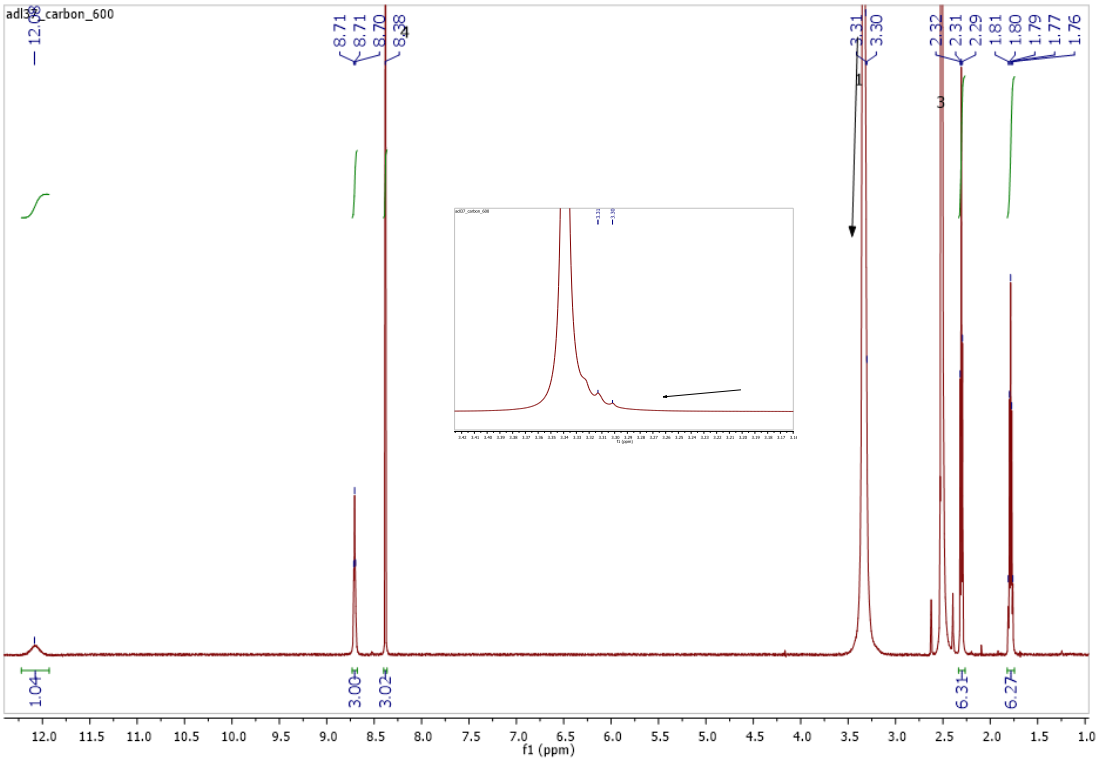

Figure S22 ^{1}H NMR spectrum of **1**

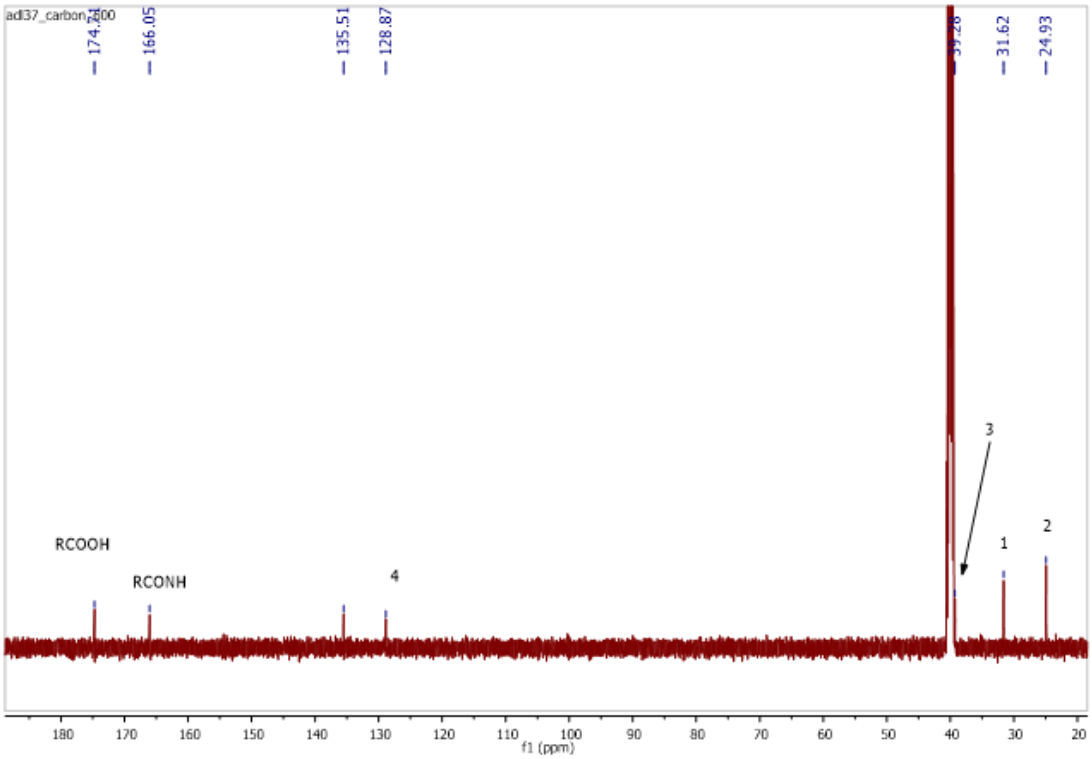

Figure S23 ^{13}C NMR spectrum of **1**

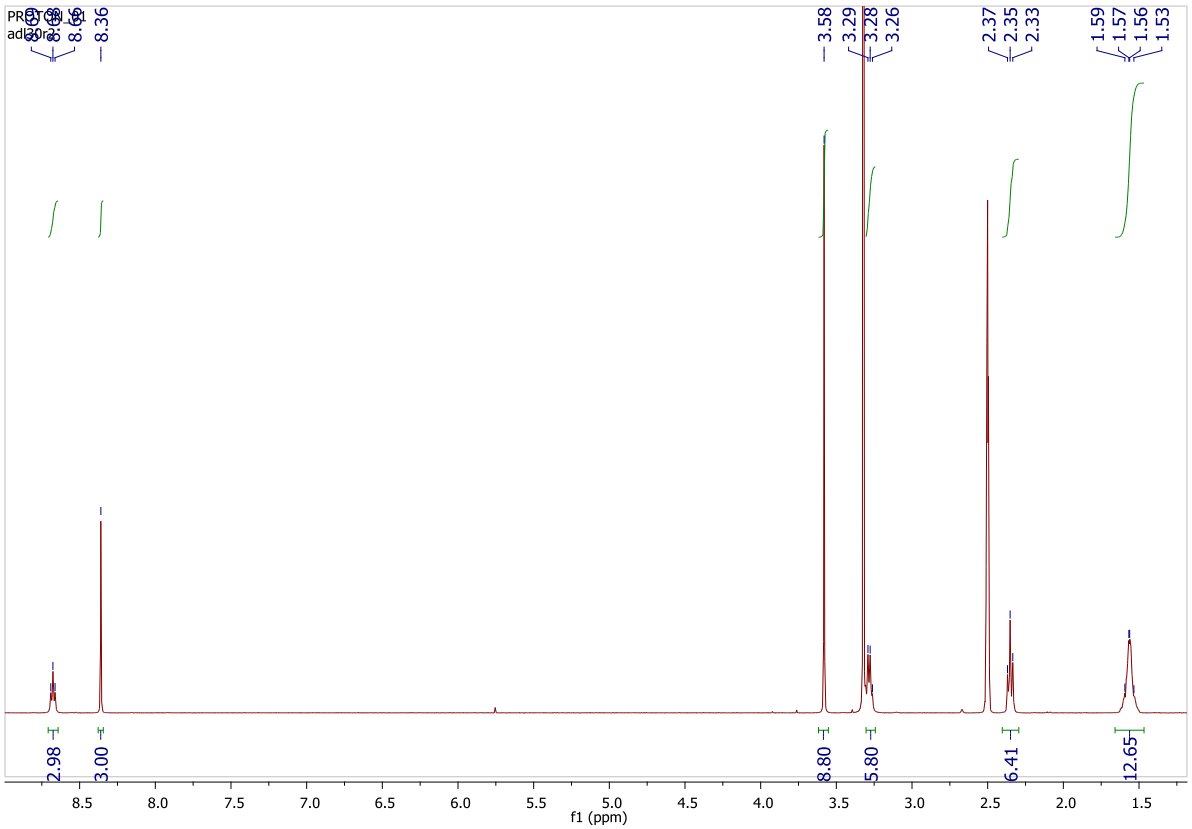

Figure S24 ^{1}H NMR spectrum of **2**

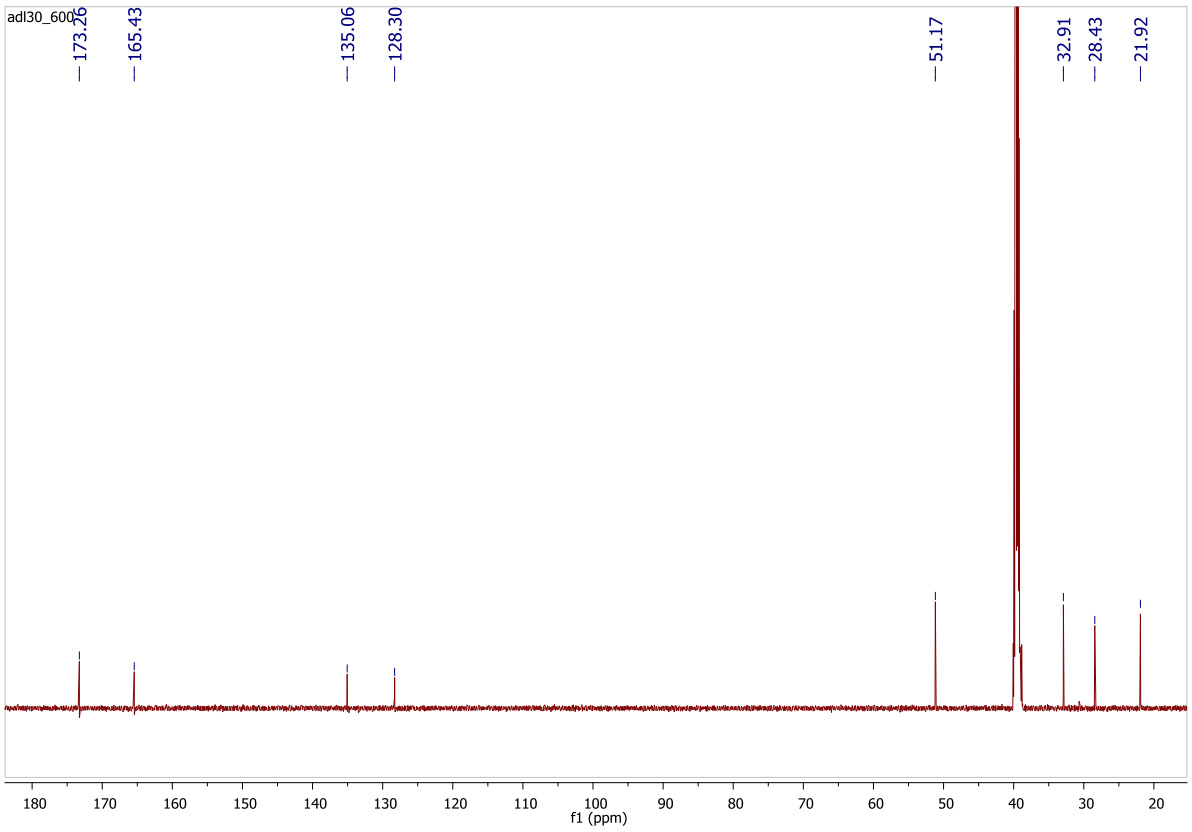

Figure S25 ^{13}C NMR spectrum of **2**

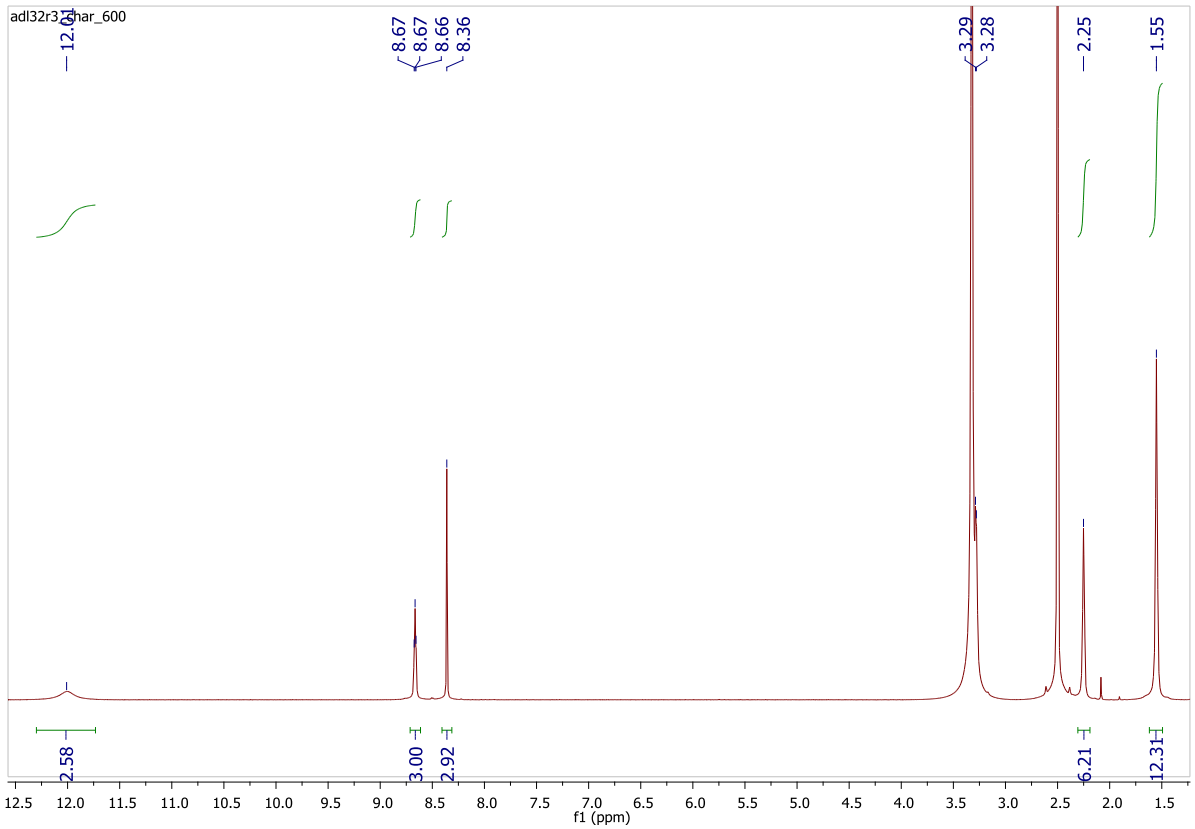

Figure S26 ^{1}H NMR spectrum of **3**

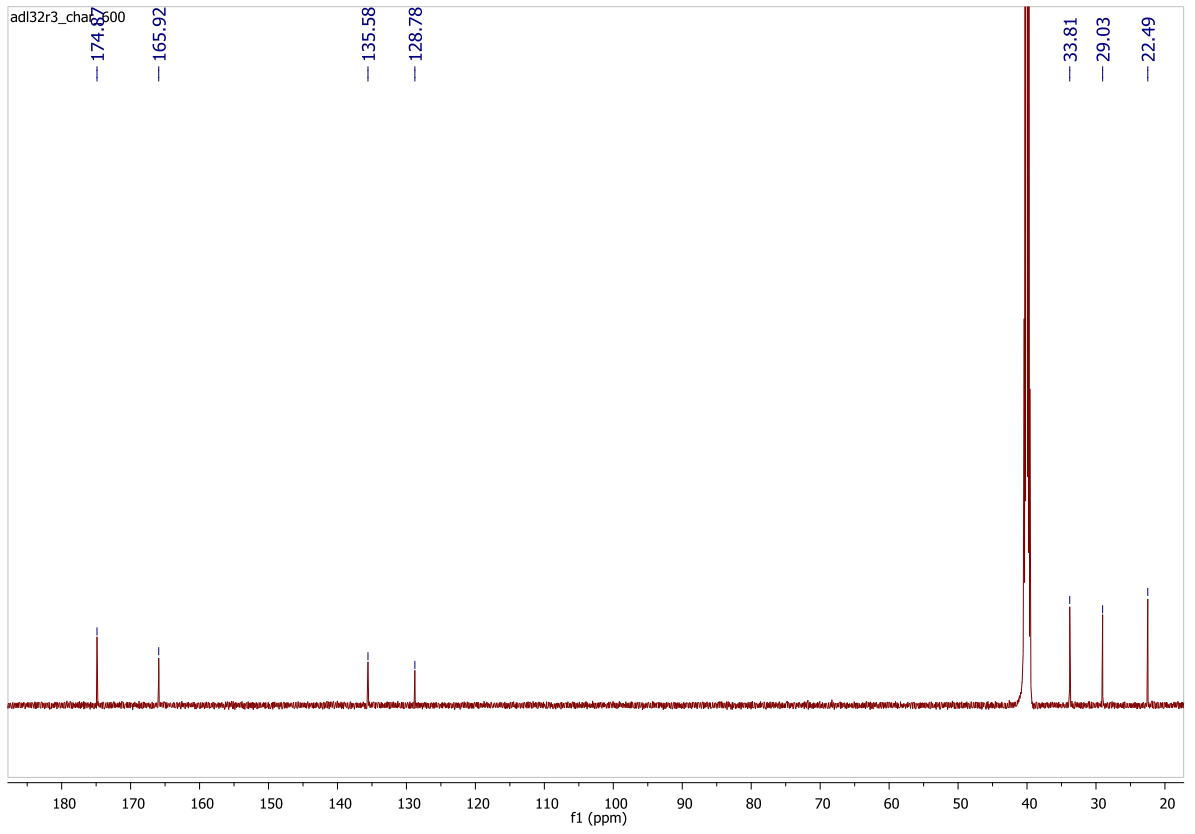

Figure S27 ^{13}C NMR spectrum of **3**

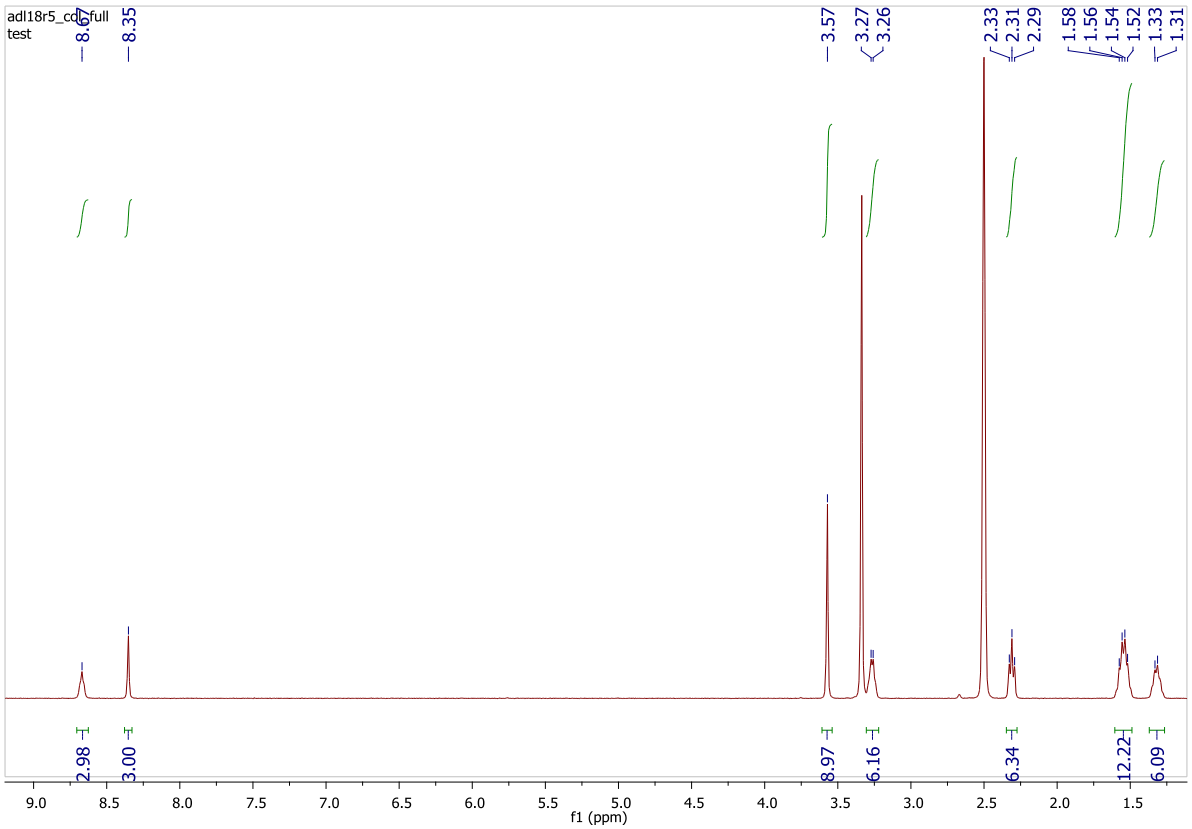

Figure S28 ^{1}H NMR spectrum of **4**

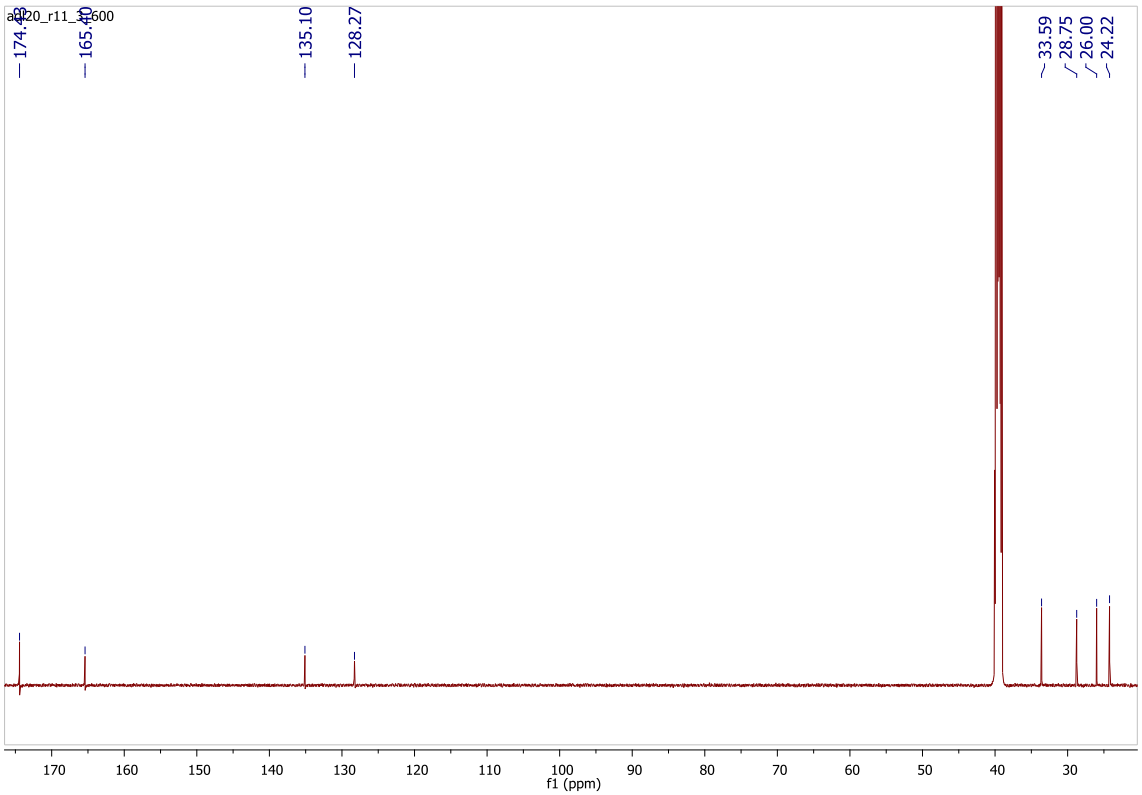

Figure S29 ^{13}C NMR spectrum of **4**

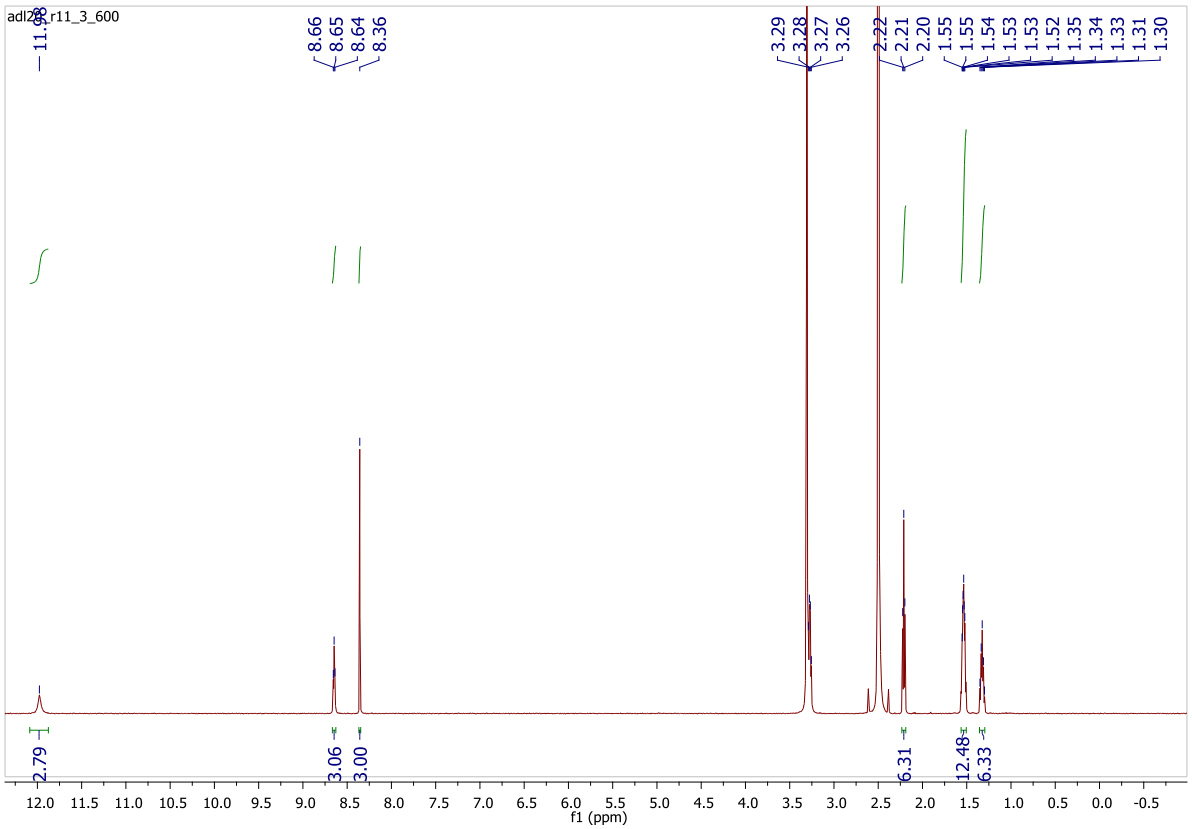

Figure S30 ^{1}H NMR spectrum of **5**

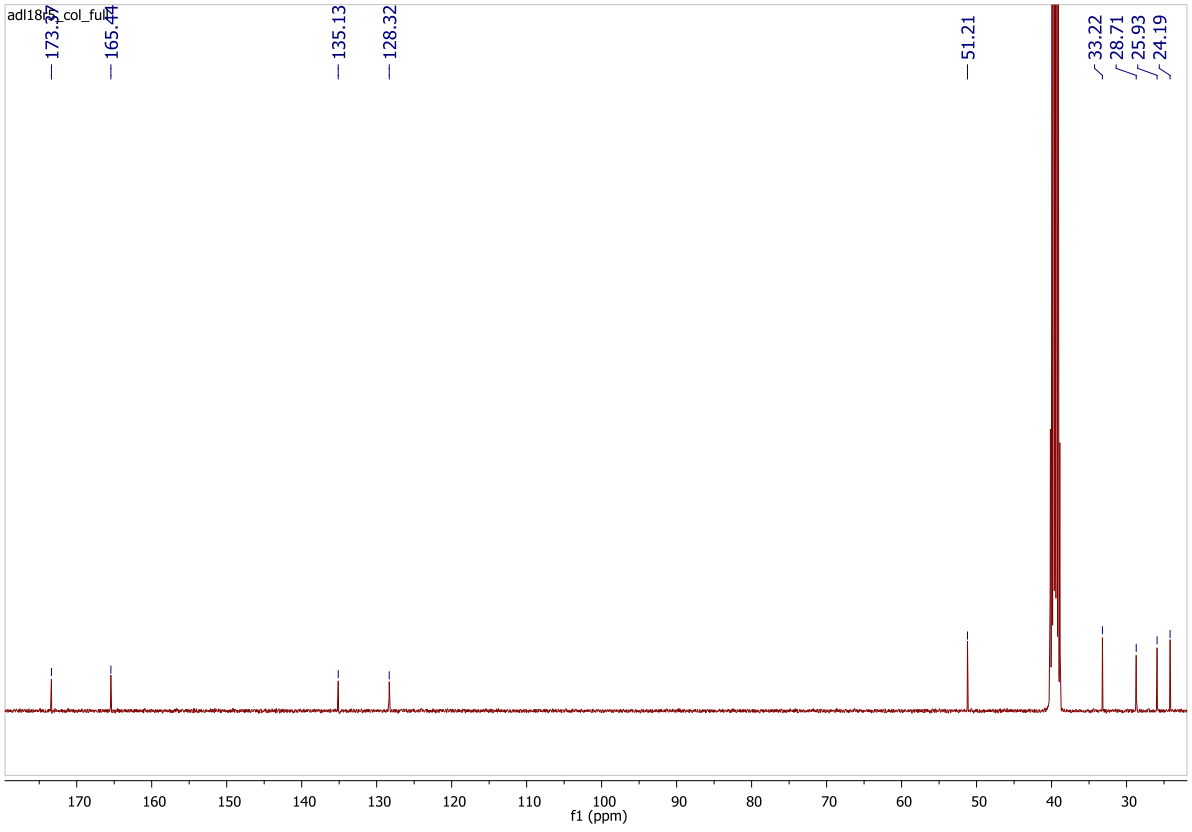

Figure S31 ^{13}C NMR spectrum of **5**

7. Additional Figures

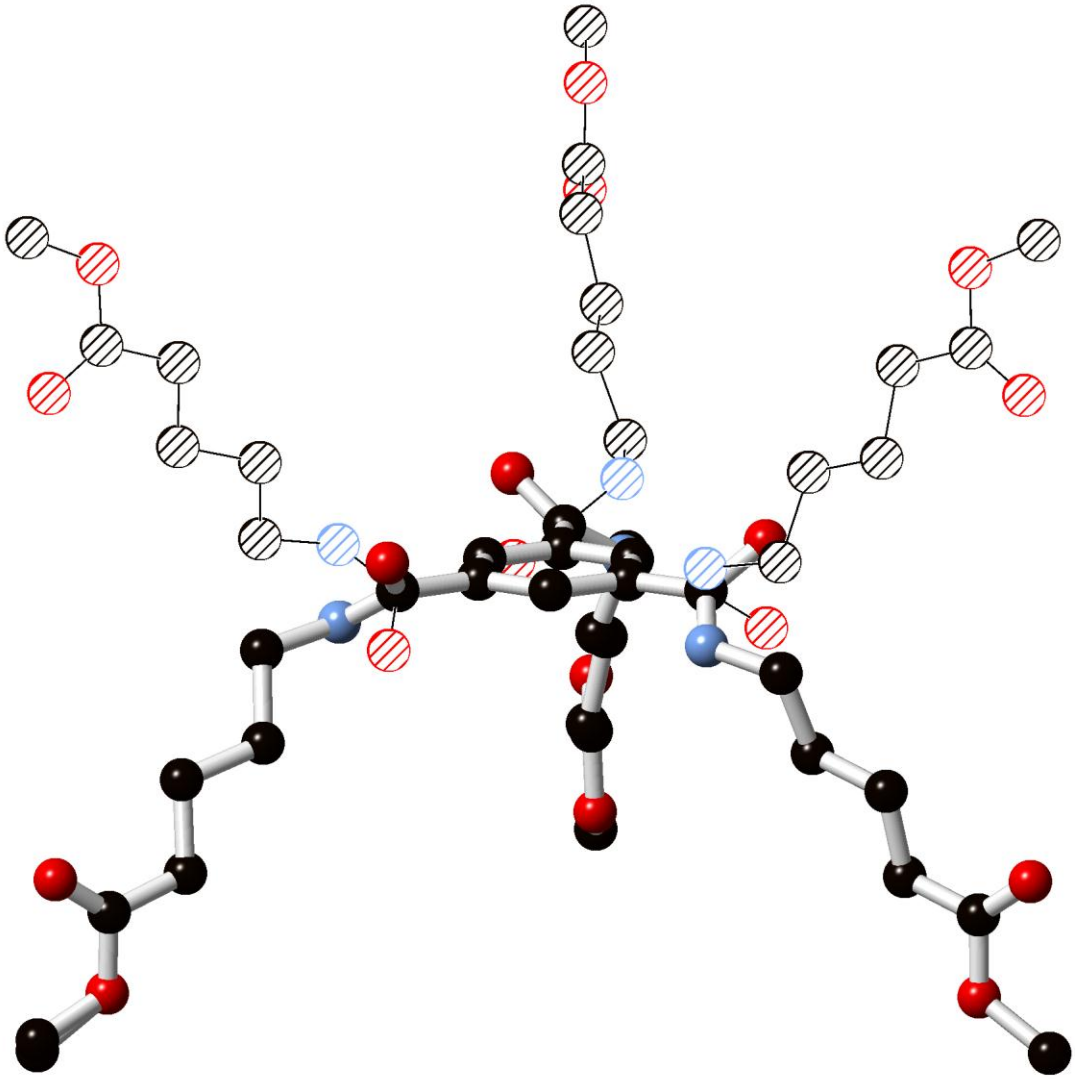

Figure S32 The two overlapping disordered orientations of compound **2**, modelled as an average across the entire structure by the mirror plane parallel to the phenyl ring.

8. References

S1. N. G. Delaney, *EP 0136883*, 1985.

S2. L. Gros, S. O. Lorente, Jimenez, V. Yardley, L. Rattray, H. Wharton, S. Little, S. L. Croft, L. M. Ruiz-Perez, D. Gonzalez-Pacanowska and I. H. Gilbert, *J. Med. Chem.*, 2006, **49**, 6094-6103.